Geotextiles and Geomembranes 46 (2018) 1–10

Contents lists available at ScienceDirect

Geotextiles and Geomembranes

journal homepage: www.elsevier.com/locate/geotexmem

Strength characteristics of soilbags under inclined loads

Si-Hong Liu [a], Fan Jia [a, *], Chao-Min Shen [a], Li-Ping Weng [b]

[a] College of Water Conservancy and Hydropower Engineering, Hohai University, Xi-Kang Road 1#, Nanjing 210098, China
[b] Business School of Hohai University, Xi-Kang Road 1#, Nanjing 210098, China

ARTICLE INFO

Article history:
Received 29 April 2017
Received in revised form
29 August 2017
Accepted 3 September 2017

Keywords:
Geosynthetics
Soilbag
Inclined load
Strength formula
DEM
Biaxial compression

ABSTRACT

The application of soilbags in permanent or semi-permanent projects is becoming increasingly wider. When used in some projects like retaining walls, soilbags are usually undertaken loads that are not perpendicular to their long axis direction, i.e. under inclined loads. In this study, a 2D strength formula of soilbags under inclined loads is derived, expressed as the apparent cohesion c_T resulting from the tensile force of the bags. A way of modeling flexible bags in DEM simulation is proposed. The soilbags stacked at different inclination under biaxial compression is numerically simulated by DEM to verify the derived strength formula of soilbags. The results indicate that under inclined loads, the developed tensile forces of the bags and thus the corresponding apparent cohesion c_T of soilbags decrease with the increasing inclination of soilbags.

1. Introduction

Soilbag, with soil contained in a bag, is familiar to everyone. For a long time, soilbags have been used to prevent a flow of soils from floodwater and build temporary structures in case of emergency (Kim et al., 2004). It is probably because of no knowledge on the features of soilbags and the deterioration of soilbags after a long exposure to sunlight, especially for such polyethylene-made soilbags that are very sensitive to ultraviolet rays. As a result of the studies by Matsuoka et al. (1999, 2000b, 2003, 2006), many advantages of soilbags, such as improving bearing capacity of soft ground, being friendly to our environment, reducing traffic-induced vibration, preventing frost heave and so on, have been elucidated. It has been found that the polythene (PE) or polypropylene (PP)-made bag is stable against both acids and alkali, and is durable if the bag is protected from the exposure to sunlight by embedding it into ground. Recently, the use of soilbags has been extended to permanent or semi-permanent projects, such as soft soil foundation reinforcement (Matsuoka and Liu, 2006; Liu and Matsuoka, 2007; Xu et al., 2008; Li et al., 2013), expansive soil treatment (Liu et al., 2012, 2015; Wang et al., 2015), base vibration isolation (Liu et al., 2014), retaining wall construction (Liu and Matsuoka, 2007; Lee et al., 2013; Wen et al., 2016), coastal protection projects (Martinelli et al., 2011; Hornsey et al., 2011; Kim et al., 2015; Moreira et al., 2016), soil railway embankment reinforcement (Matsuoka and Liu, 2006; Indraratna et al., 2014; Liu et al., 2017) and so on.

In the case of reinforcing soft building foundation, soilbags are mainly subjected to vertical loads from the upper structure weight (parallel to the short axis of soilbags); while in the case of constructing retaining walls, soilbags bear backfill earth pressures that are inclined to the vertical direction (not parallel to the short axis of soilbags), as indicated in Fig. 1. In this study, we define the angle between the direction of the major principal stress σ_1 and the short axis of soilbag as δ. Thus, in the case of reinforcing soft building foundation, the angle $\delta = 0$.

So far, many researches on the compressive strength of the soilbag in the case of $\delta = 0$ have been conducted. Matsuoka et al. (2000a, 2003, 2006) derived a strength formula of the soilbag in two dimensional stress states (2D) and verified it through a series of unconfined and biaxial compression tests, in which the high compressive strength of the soilbag was interpreted as the contribution of an apparent cohesion c resulting from the tension of the bag. Based on the generalized Mises and the Lade-Duncan failure criteria, Bai et al. (2010) suggested two compressive strength formulas of the soilbag in three-dimensional stress states, which can predict the compressive strength of soilbags under vertical loads

* Corresponding author.
E-mail addresses: sihongliu@hhu.edu.cn (S.-H. Liu), kv@hhu.edu.cn, jiafan_kv@163.com (F. Jia), chaomin.shen@hotmail.fr (C.-M. Shen), wlp@hhu.edu.cn (L.-P. Weng).

http://dx.doi.org/10.1016/j.geotexmem.2017.09.002
0266-1144/

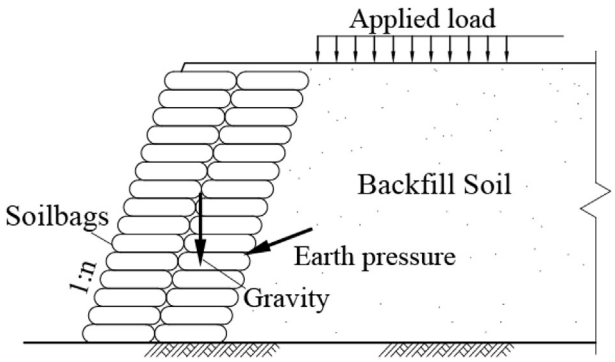

Fig. 1. Construction of retaining wall with soilbags.

more accurately. On the other hand, some numerical analyses have also been carried out on soilbags in the case of $\delta = 0$. The effectiveness of the ground improvement with soilbags has been validated as the result of the finite element analysis (Muramatsu et al., 2007; Tantono and Bauer, 2008; Ansari et al., 2011). The FEM simulation conducted by Ye et al. (2011) showed that soilbags could greatly reduce the ground vibration propagated from a point vibration source. And some numerical modeling of geosynthetics has been conducted using the DEM and proper coupling between the DEM and other methods (Bhandari and Han, 2010, 2015; Ahmed et al., 2015; Ngo et al., 2015; Chen et al., 2015; Cheng et al., 2017). By using the distinct element method (DEM), Cheng et al. (2016) numerically investigated the stress states and fabric anisotropies in the wrapped soil under unconfined compression and simple shear. The performance and mechanisms of the soilbag earth reinforcement method, i.e., confinement and interlocking, can be better understood from the perspectives of stress state, volumetric change and anisotropies.

When soilbags are used to construct permanent structures like retaining walls, they may be subjected to external loads not parallel to the short axis of soilbag, i.e. $\delta \neq 0$. In this paper, we present a 2D strength formula of the soilbag in the case of $\delta \neq 0$ and the verification through the numerical simulation using distinct element method (DEM).

2. Strength of soilbags in the case of $\delta = 0$

First, we review the 2D strength formula of the soilbag derived by Matsuoka et al. (2000a, 2003, 2006). Fig. 2 (a) shows a soilbag subjected to external principal stresses σ_1 and σ_3 in a two-dimensional manner. Under the actions of σ_1 and σ_3, the soilbag usually tends to be flat, accompanied by the extension of the total perimeter of the bag. As a result, a tensile force T is produced along the bag, which in turn produces an additional stress on the soil particles inside the bag. The components of the additional stress are expressed as

$$\sigma_{01} = 2T/(B \times 1); \quad \sigma_{03} = 2T/(H \times 1) \tag{1}$$

where B and H are the width and height of the soilbag, respectively. Thus, the stresses acting on the soil wrapped in the bag are the combined result of the externally applied stresses and the apparently produced stresses by the bag tensile force T, as shown in Fig. 2 (b). At failure, the following equation holds:

$$\sigma_1 + \frac{2T}{B} = K_p\left(\sigma_3 + \frac{2T}{H}\right) \tag{2}$$

where $K_p = (1 + \sin\varphi)/(1 - \sin\varphi)$ and φ is the internal angle of

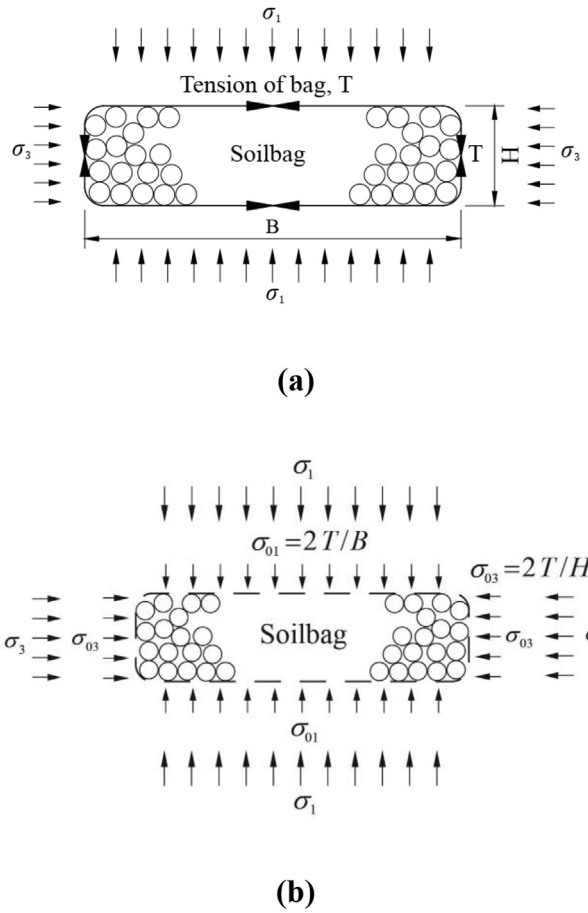

Fig. 2. Stresses acting on two-dimensional model soilbag and on particles inside the soilbag: (a) Stresses acting on soilbag; (b) Stresses acting on particles inside soilbag.

friction of the wrapped soil. As the width B is usually greater than the height H for soilbag, it is known from Eq. (1) that the tensile force T induced along the bag causes stronger confinement to the wrapped soil in the σ_3 direction than in the σ_1 direction. Thus, the larger the ratio of B/H of the soilbag is, the more the reinforcement effect is.

By comparing Eq. (2) with the strength expression of $\sigma_1 = \sigma_3 K_p + 2c\sqrt{K_p}$ for a cohesive-frictional material, the following expression of the apparent cohesion, c, of the soilbag resulting from the bag tension T is obtained.

$$c_T(\delta = 0) = \frac{T}{B\sqrt{K_p}}\left(\frac{B}{H}K_p - 1\right) \tag{3}$$

Thus, soilbag can be taken as a cohesive-frictional material with an apparent cohesion c as expressed in Eq. (3) and the same internal friction angle φ as that of the material contained in the bag. That is to say, the high compressive strength of the soilbag can be interpreted as the contribution of an apparent cohesion c resulting from the tension of the bag.

3. Strength of soilbags in the case of $\delta \neq 0$

Fig. 3 shows a two-dimensional soilbag that is inclined to the horizontal direction with an angle of δ, but subjected to the vertical major principal stress σ_1 and the horizontal minor principal stress σ_3. For the case of $\delta \neq 0$, through a series of biaxial compression tests on the wrapped aluminum rod assemblies, Matsuoka and Liu

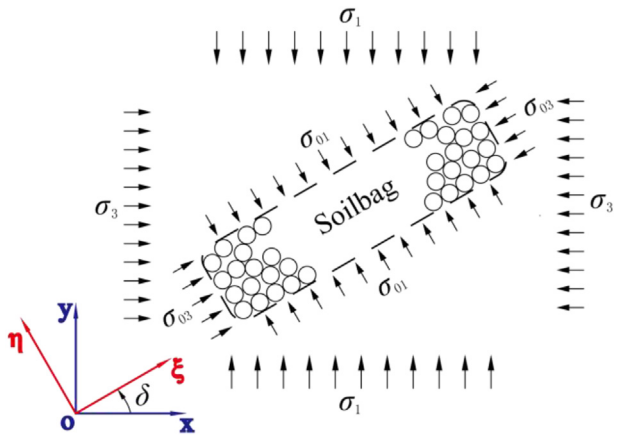

Fig. 3. Soilbag inclined to externally applied stress with an angle of δ.

(2006) suggested an empirical equation of the apparent cohesion of soilbags, expressed as

$$c_T(\delta) = \begin{cases} c_T(\delta = 0)\cdot\cos 2\,\delta & (0 \le \delta \le 45^\circ) \\ 0 & (45^\circ \le \delta \le 90^\circ) \end{cases} \tag{4}$$

However, the mathematical and theoretical meaning of the above equation has not been elucidated. Hereinafter, we will derive a strength equation of the soilbag under inclined loads. The derivation is based on the following two assumptions:

(i) The soilbag is mainly compressed under the externally applied σ_1 and σ_3 that will take place when the inclined angle δ is not so large. As aforementioned, the perimeter of the compressed soilbag will be elongated. As a result, a tensile force T will be produced along the bag, which in turn produces an additional stress acting on the wrapped soil.
(ii) The slippage between soilbags is not considered. That is to say, the failure of the soilbag results from the failure of the wrapped soil, which is governed by the Mohr-Coulomb failure criterion.

In the case of $\delta \neq 0$, the externally applied stress (σ_1, σ_3) can be divided into two components: one is normal to the soilbag surface, and the other is tangential to the soilbag surface. According to the assumption (i), the effect of the tangential components on the tensile force T is ignored. Thus, the components of the additional stress $(\sigma_{01}, \sigma_{03})$ resulting from the tensile force T of the bag are still calculated by using Eq. (1). The direction of the additional stress is inclined to the direction of the externally applied stress with the same angle of δ.

We define $\mathbf{x}, y$ the directions of the externally applied stress σ_3 and σ_1, respectively. Similarly, ξ, η are defined as the directions of the additional stress σ_{03} and σ_{01}, respectively. The angle between the two bases is δ, as shown in Fig. 3.

For the soilbag under the biaxial compression, the stress of the soil wrapped in the bag $\boldsymbol{\sigma_s}$ is the sum of the externally applied stress $\boldsymbol{\sigma}$ and the additional stress produced by the tension of the bag $\boldsymbol{\sigma_T}$:

$$\boldsymbol{\sigma_s} = \boldsymbol{\sigma} + \boldsymbol{\sigma_T} \tag{5}$$

The matrix form of the externally applied stress $\boldsymbol{\sigma}$ in the xy coordinate system is:

$$\boldsymbol{\sigma} = \begin{bmatrix} \sigma_3 & 0 \\ 0 & \sigma_1 \end{bmatrix}_{(x,y)} \tag{6}$$

And the matrix form of the additional stress produced by the tension of the bag $\boldsymbol{\sigma_T}$ in the $\xi\eta$ coordinate system is:

$$\boldsymbol{\sigma_T} = \begin{bmatrix} \frac{2T}{H} & 0 \\ 0 & \frac{2T}{B} \end{bmatrix}_{(\zeta,\eta)} \tag{7}$$

Through the base transformation, in the xy coordinate system $\boldsymbol{\sigma_T}$ is rewritten as:

$$\boldsymbol{\sigma_T} = \begin{pmatrix} \frac{2T}{H}\cos^2\delta + \frac{2T}{B}\sin^2\delta & \left(\frac{2T}{H} - \frac{2T}{B}\right)\sin\delta\cos\delta \\ \left(\frac{2T}{H} - \frac{2T}{B}\right)\sin\delta\cos\delta & \frac{2T}{H}\sin^2\delta + \frac{2T}{B}\cos^2\delta \end{pmatrix}_{(x,y)} \tag{8}$$

By substituting Eq. (6) and Eq. (8) into Eq. (5), one can obtain the stress of the soil wrapped in the bag $\boldsymbol{\sigma_s}$:

$$\boldsymbol{\sigma_s} = \begin{pmatrix} \sigma_3 + \frac{2T}{H}\cos^2\delta + \frac{2T}{B}\sin^2\delta & \left(\frac{2T}{H} - \frac{2T}{B}\right)\sin\delta\cos\delta \\ \left(\frac{2T}{H} - \frac{2T}{B}\right)\sin\delta\cos\delta & \sigma_1 + \frac{2T}{H}\sin^2\delta + \frac{2T}{B}\cos^2\delta \end{pmatrix}_{(x,y)} \tag{9}$$

According to the assumption (ii), the failure of the soilbag is caused by the shear failure of the wrapped soil, which is governed by the Mohr-Coulomb failure criterion. It is expressed in terms of the major and minor principal stresses as:

$$\frac{\sigma_{1s} - \sigma_{3s}}{2} = \frac{\sigma_{1s} + \sigma_{3s}}{2}\sin\varphi_s + c_s\cos\varphi_s \tag{10}$$

where σ_{1s} and σ_{3s} are the major and minor principal stresses of the wrapped soil, respectively; c_s and φ_s are the cohesion and the internal friction angle of the wrapped soil, respectively.

σ_{1s} and σ_{3s} can be calculated from the eigenvalues of the stress tensor $\boldsymbol{\sigma_s}$ in Eq. (9). Substituting them into Eq. (10) yields:

$$\left(\frac{\sigma_1 - \sigma_3}{2}\right)^2 - (\sigma_1 - \sigma_3)\left(\frac{T}{H} - \frac{T}{B}\right)\cos 2\,\delta + \left(\frac{T}{H} - \frac{T}{B}\right)^2 = \left[\left(\frac{\sigma_1 + \sigma_3}{2} + \frac{T}{H} + \frac{T}{B}\right)\sin\varphi_s + c_s\cos\varphi_s\right]^2 \tag{11}$$

Usually, the strength envelop of soilbags represents the relation between $(\sigma_1 - \sigma_3)/2$ and $(\sigma_1 + \sigma_3)/2$. Fig. 4 shows the strength

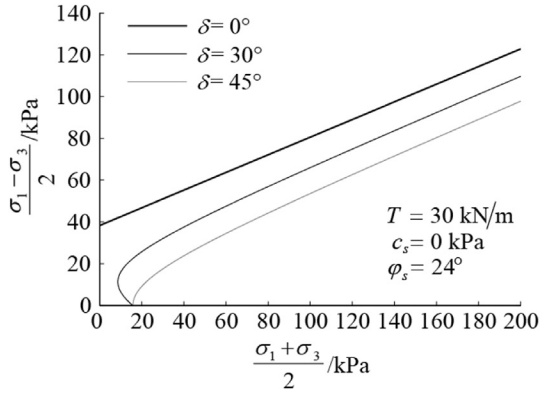

Fig. 4. The strength envelops of soilbags at three different inclined angles calculated by Eq. (11).

envelops of soilbags at three different inclined angles δ calculated by Eq. (11) under the condition of $T = 30$N, $\varphi_s = 24°$and $c_s = 0$. It can be seen that the strength envelops of soilbags in the case of $\delta \neq 0$ correspond to hyperbolic curves. Thus, Eq. (11) can be rewritten as the following hyperbolic standard form:

$$\frac{\left[\frac{\sigma_1+\sigma_3}{2}+\frac{T}{H}+\frac{T}{B}+c_s\cot\varphi_s\right]^2}{\frac{(1-\cos^2 2\delta)\left(\frac{T}{H}-\frac{T}{B}\right)^2}{\sin^2\varphi_s}}-\frac{\left[\frac{\sigma_1-\sigma_3}{2}-\left(\frac{T}{H}-\frac{T}{B}\right)\cos 2\,\delta\right]^2}{(1-\cos^2 2\delta)\left(\frac{T}{H}-\frac{T}{B}\right)^2}=1 \tag{12}$$

For the sake of simplicity, the strength envelop of soilbags is approximated by the asymptote of the hyperbolic curve. The asymptote of Eq. (12) is calculated to be

$$\frac{\sigma_1-\sigma_3}{2}=\frac{\sigma_1+\sigma_3}{2}\sin\varphi_s+(m+1)\frac{T}{B}\sin\varphi_s+c_s\cos\varphi_s+(m-1)\frac{T}{B}\cos 2\,\delta \tag{13}$$

in which m = B/H. Compared with the Mohr-Coulomb failure criterion, the apparent cohesion c_T of the soilbag produced by the tensile force T under inclined loads can be obtained from Eq. (13):

$$c_T=(m+1)\frac{T}{B}\tan\varphi_s+(m-1)\frac{T}{B}\frac{\cos 2\,\delta}{\cos\varphi_s} \tag{14}$$

In Eq. (14), the tensile force T of the bag changes with the inclined angle δ, which is assumed to be

$$T=\lambda(\delta)T_v \tag{15}$$

where $\lambda(\delta)$ is a reduction factor ranging from 1 to 0. When the inclined angle $\delta = 0$, $\lambda(\delta) = 1$. T_v is the tensile force of the bag in the case of $\delta = 0$ when the failure of the wrapped soil happens.

Finally, the apparent cohesion c_T of soilbags produced by the tensile force T under inclined loads is obtained by substituting Eq. (15) into Eq. (14).

$$c_T=(m+1)\frac{\lambda(\delta)T_v}{B}\tan\varphi_s+(m-1)\frac{\lambda(\delta)T_v}{B}\frac{\cos 2\,\delta}{\cos\varphi_s} \tag{16}$$

As stated above, $\lambda(\delta) = 1$ when the inclined angle $\delta = 0$. In this case, Eq. (16) becomes

$$c_T=(m+1)\frac{T_v}{B}\tan\varphi_s+\frac{1}{\cos\varphi_s}(m-1)\frac{T_v}{B} \tag{17}$$

It can be justified that Eq. (17) is the same as Eq. (3) despite they are expressed in a different way.

4. DEM analysis of biaxial compression tests on soilbags

In sections 2 and 3, the strength formula of soilbags in the cases of both $\delta = 0$ and $\delta \neq 0$ have been derived on the basis of the Mohr-Coulomb failure criterion. Next, the biaxial compression tests on soilbags will be numerically analyzed by using distinct element method (DEM) to verify the derived strength formula of soilbags.

4.1. Outline of DEM analysis

Only a brief introduction to two-dimensional distinct element method (DEM), pioneered by Cundall (1971) and Cundall and Strack (1979), is given here. DEM is a numerical technique in which individual particles are represented as rigid bodies. In two dimensions each particle has three degrees of freedom (two translations and one rotation). Each particle can be in contact with neighboring particles or structure boundaries. The contact between two particles, or a particle and a boundary, is modeled by a spring and dashpot in both the normal and tangential directions (*see* Fig. 5). The normal direction spring has a no-tension constraint. In the tangential direction, if the tangential force reaches a Coulomb friction limit, it is allowed to slide. Small amounts of viscous damping are often included to help provide dissipation of high-frequency motion. The forces generated at a contact are computed based on the overlap of the bodies at the contact and the stiffness of the springs, which are then used to compute the acceleration of the body according to Newton's laws of motion. After the acceleration is determined, new velocity and displacement for the particle is computed using the central difference explicit time integration. To ensure the convergence of the numerical solution, the time step Δt is taken to be $1/10\Delta t_c$, where Δt_c is the critical time step. The critical time step is estimated on the basis of the single degree-of-freedom system of a mass m connected to ground by a spring of stiffness k, for which the critical time step Δt_c equals $2\sqrt{m/k}$. With the newly computed displacement configuration, the state of deformation at the existing contacts is re-evaluated, and the possible creation of new contacts is evaluated, leading to a new cycle of computation.

4.2. Modeling flexible bag

In the contact model shown in Fig. 5, forces between particles are generated only when they are in contact. The normal direction spring has a no-tension constraint. Obviously, this model is not suitable for the flexible bag that takes effect only when extended and cannot withstand compression. In this study, the flexible bag is modeled as follows (Fig. 6):

(i) Around the circumference of the bag, very small mono-sized circular particles, termed as bag particles in this paper for convenience, are arranged, as shown in Fig. 6. The distance between any two neighboring bag particles is small enough to prevent the outward escape of the particles contained in the bag.

(ii) Two neighboring bag particles are connected in their normal direction (connection of the two particle centers) with an elastic spring and a viscous dashpot, but not connected in their tangential direction to model the flexibility of the bag, as shown in Fig. 6. When the distance between two neighboring bag particles is elongated, a tensile force is generated, which is computed based on the elongated distance and the stiffness of the spring. The computed tensile force is set to be zero if it exceeds the tensile strength of the bag. If two

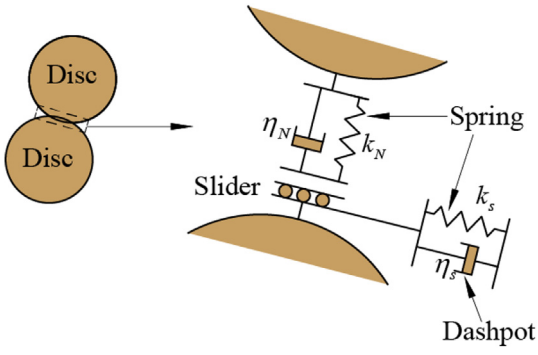

Fig. 5. Contact model for particles inside soilbags used in DEM simulation.

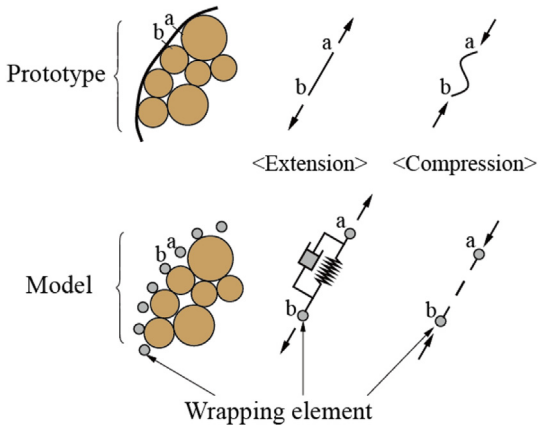

Fig. 6. Modeling flexible bag in DEM simulation.

neighboring bag particles at a time step come to be close, then no any forces are generated between them.

(iii) The interaction between the bag particle and the bag-wrapped particle is the same as that between two bag-wrapped particles, i.e. modeling with a spring and dashpot in both the normal and the tangential directions (*see* Fig. 5). While the friction μ of bag particle-bag particle, particle-bag particle and bag particle-wall is assumed to be zero because the bag in this study is idealized as a flexible-perfectly material.

4.3. Simulation of biaxial compression tests

Firstly, a DEM model of one soilbag with a width B of 40 cm and a height H of 10 cm was generated. The model is made up of 921 circular particles with diameters randomly ranging from 4 mm to 16 mm and 480 mono-sized bag particles with a diameter of 0.9 mm. Then, the DEM specimen for the biaxial compression test was built. One DEM specimen contains three model soilbags, which are stacked at different inclined angles (δ=0°, 5°, 15°, 30°, 45°). For any inclined angle δ, the DEM specimen is bounded by four rigid walls (two horizontal and two vertical) and the space between the stacked soilbags and the rigid walls is filled with the same particles as in the bag, as shown in Fig. 7.

The input parameters used in the DEM simulation are summarized in Table 1. The time increment Δt is taken to be 5×10^{-7}s. The stiffness (k_n, k_s) and damping η_n, η_s in Table 1 were determined from the contact theory of two elastic discs. And the inter-particle friction μ was obtained from the frictional tests on aluminum rods by Matsuoka and Yamamoto (1994). These parameters have been used to simulate biaxial compression, simple shear and direct shear tests on an assembly of aluminum rods, and the simulated results agreed very well with the actual experimental results (Yamamoto, 1995; Liu and Lu, 2000; Liu and Xu, 2001; Liu and Sun, 2002; Liu and Matsuoka, 2003; Liu, 2006).

The numerical biaxial compression tests on soilbags stacked with one inclined angle were carried out at the confining stresses of 100 kPa, 200 kPa and 300 kPa, respectively. The DEM specimen was loaded by lowering the top wall at a constant rate of 1 cm/s while the bottom wall was fixed and the two side walls were servo-controlled to maintain a constant confining stress.

4.4. Results and discussion

Fig. 8 gives the numerically simulated stress-strain relations of soilbags at three different inclined angles δ of 0°, 30° and 45°. As shown in Fig. 8 (a), in the case of $\delta = 0°$, the failure of the two specimens under the confining stresses σ_3 of 200 kPa and 300 kPa results from the breakage of the bags, accompanying with the rapid decrease of the deviatoric stress $(\sigma_1 - \sigma_3)$. The shear strengths of the two specimens were taken as the deviatoric stresses at the bag-broken points. Apart from these two specimens, the bags of the other specimens keep effect during shearing. The deviatoric stresses $(\sigma_1 - \sigma_3)$ of them increase and gradually tend to a stable value as the vertical compression continues to a strain ε_1 of 15%. The shear strengths of the specimens were taken from the peak values of the deviatoric stresses during shearing. Based on the simulation results, the Mohr's stress diagrams and the shear strength envelops of the soilbags in the cases of $\delta = 0°$, 30° and 45° are drawn in Fig. 9. It can be seen from Fig. 9 that in the cases of $\delta = 0°$, 30° and 45°, the apparent cohesions c of the soilbags are 88 kPa, 25 kPa and 5 kPa, respectively, with a constant internal friction angle $\varphi = 24°$. By the way, the biaxial compression tests on the same particles as wrapped inside the bags were also simulated by using the parameters in Table 1. The obtained internal friction angle of the particles is about 24°. In Fig. 9, the internal friction

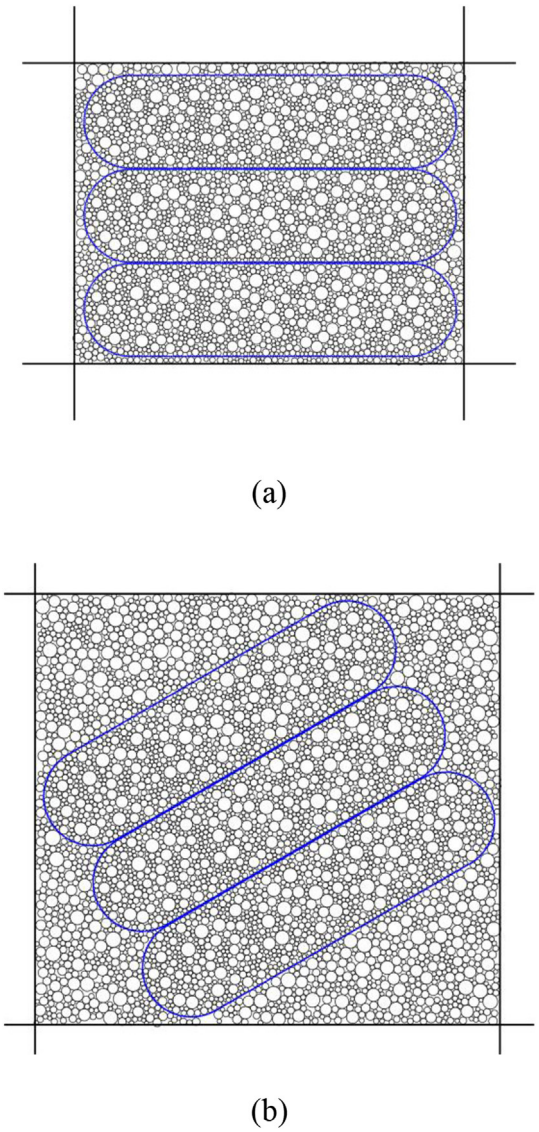

Fig. 7. DEM specimens of biaxial compression tests on soilbags: (a) $\delta = 0°$; (b) $\delta \neq 0°$.

Table 1
Input parameters used in DEM simulation.

	Particle- particle	Bag particle- bag particle	Particle- bag particle	Particle- wall	Bag particle- wall
k_n (N/m/m)	9.0×10^9	9.0×10^8	9.0×10^8	1.8×10^{10}	1.8×10^9
k_s (N/m/m)	1.2×10^8	0	1.4×10^7	2.4×10^8	2.8×10^7
η_n (N s/m/m)	7.9×10^4	4.3×10^3	2.5×10^3	1.1×10^5	3.5×10^4
η_s (N s/m/m)	9.0×10^3	0	1.2×10^4	1.2×10^4	4.3×10^2
μ	0.29	0	0	0.29	0
ρ (kg/m^3)	2700	2700	2700	2700	2700

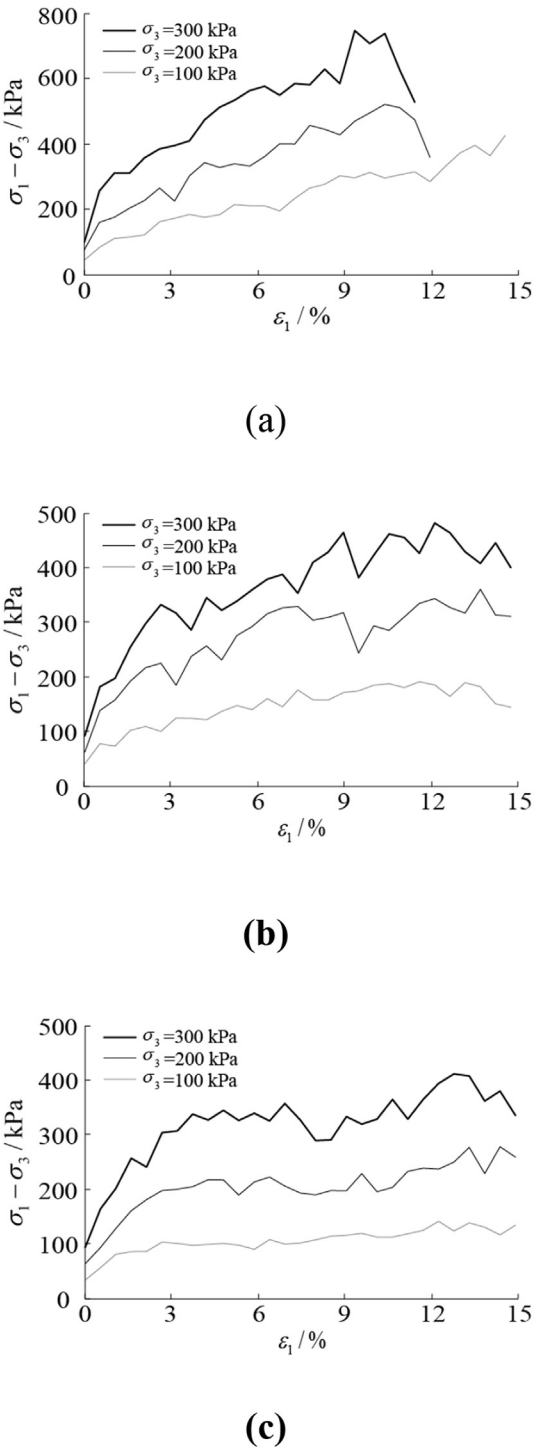

Fig. 8. Numerically simulated stress-strain relations of soilbags at different inclined angles δ: (a) $\delta = 0°$; (b) $\delta = 30°$; (c) $\delta = 45°$.

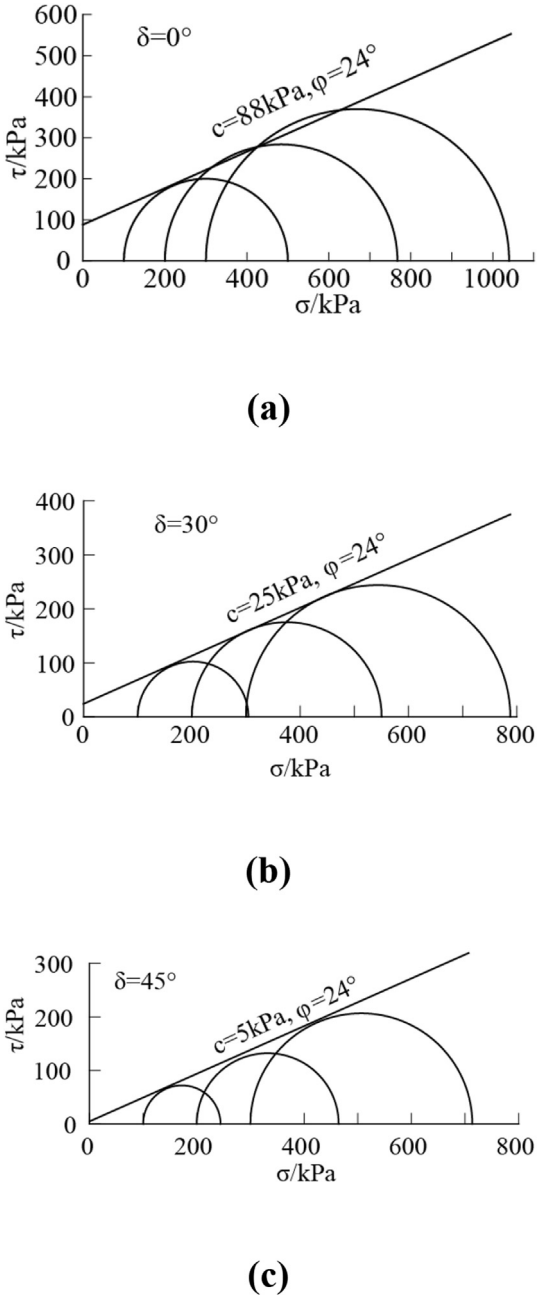

Fig. 9. The strength envelops of soilbags at different inclined angles δ: (a) $\delta = 0°$; (b) $\delta = 30°$; (c) $\delta = 45°$.

angle of the soilbags is assumed to be the same as that of the particles wrapped inside the bags. The decrease of the apparent cohesions c of the soilbags with the increasing inclined angles δ

indicates that the confinement effect of soilbags decreases gradually. It can also be observed from the distribution of the inter-particle contact forces of the soilbags as shown in Fig. 10. The thickness of the lines in Fig. 10 represents the magnitude of contact forces. In the case of $\delta = 0^\circ$, the inter-particle contact forces inside the soilbags are generally larger than those of the surrounding particles owing to the confinement effect of the bags. As the inclined angle δ reaches 45°, the inter-particle contact forces inside the soilbags are basically the same as those of the surrounding particles, indicating the confinement effect of the bags almost vanishes.

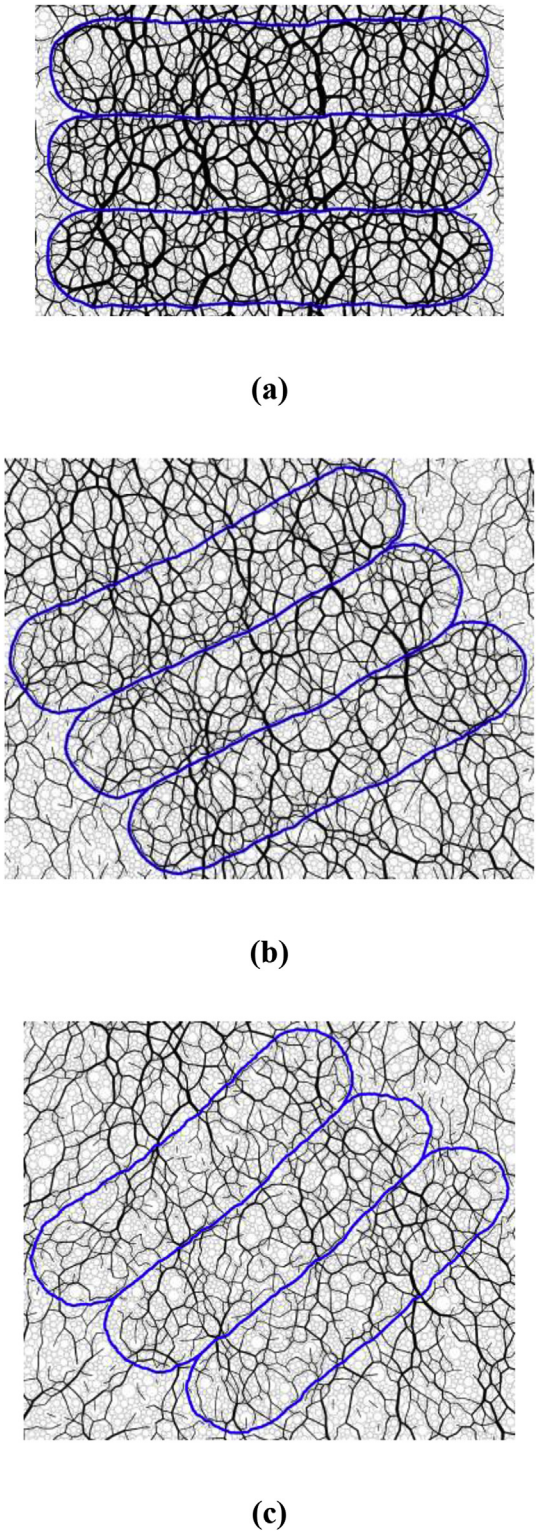

Fig. 10. The inter-particle contact forces of inclined soilbags at the end of shearing ($\varepsilon_1 = 15\%$) when $\sigma_3 = 100$kPa: (a) $\delta = 0^\circ$; (b) $\delta = 30^\circ$; (c) $\delta = 45^\circ$.

The confinement effect of the bag is quantified by the tensile force around its circumference. Fig. 11 presents the distributions of the tensile forces around the circumferences of the mid bags in the cases of three different inclined angles at $\varepsilon_1 = 8\%$ when $\sigma_3 = 100$ kPa. It can be seen that the tensile force around the circumference for a certain inclined angle is nearly uniform, and is larger at lower inclined angle. The slight fluctuation along the bag circumference is caused by the microstructure considered for modeling the bag material.

Fig. 12 gives the evolution of the tensile forces T of the bags at different inclined angles during biaxial compression under three confining stresses (σ_3=100 kPa, 200 kPa, 300 kPa), where the tensile force is taken as the average of the tensile forces around the circumferences of the bags. It can be seen that the tensile forces of the bags increase almost linearly during the biaxial compression.

In Eq. (15), the reduction factor λ is defined as the ratio of the tensile force of the bag at inclined angle ($\delta \neq 0$) to the tensile force of the bag in the case of $\delta = 0^\circ$. Fig. 13 shows the evolution of the reduction factors λ at $\delta = 30^\circ$ and $\delta = 45^\circ$ under three different confining stresses. It can be seen that the reduction factor λ decreases significantly at the beginning of the biaxial compression and gradually tends to be a stable value at an inclined angle. Moreover, the stabilized value of λ for an inclined angle is almost independent of the confining stress. The mean values of the stabilized reduction factors λ under three confining stresses (σ_3=100 kPa, 200 kPa, 300 kPa) are about 0.47 at $\delta = 30^\circ$ and 0.13 at $\delta = 45^\circ$, respectively.

In this study, we simulated the biaxial compression tests on the stacked soilbags with five different inclined angles (δ=0°, 5°, 15°, 30°, 45°). The reduction factors λ obtained from the simulations are plotted against the inclined angles δ in Fig. 14. They may be nearly fitted as

$$\lambda(\delta) = \cos(2\delta) \tag{18}$$

The selection of this fitting trigonometric function is to eliminate the effect of the dimension of the inclined angle δ. The value of the trigonometric function ranges from 1.0 to 0 when the inclined angle increases from 0° to 45°, which is in a good agreement with the variation of the simulated reduction factors.

By substituting Eq. (18) into Eq. (16), one can obtain the apparent cohesion of the soilbags under inclined loads:

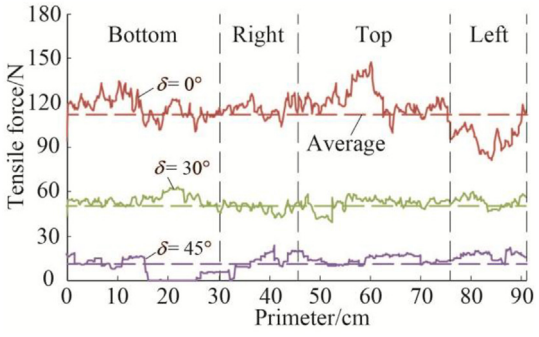

Fig. 11. Distributions of the tensile forces around the circumferences of the mid bags for different inclined angles at $\varepsilon_1 = 15\%$ when $\sigma_3 = 100$ kPa.

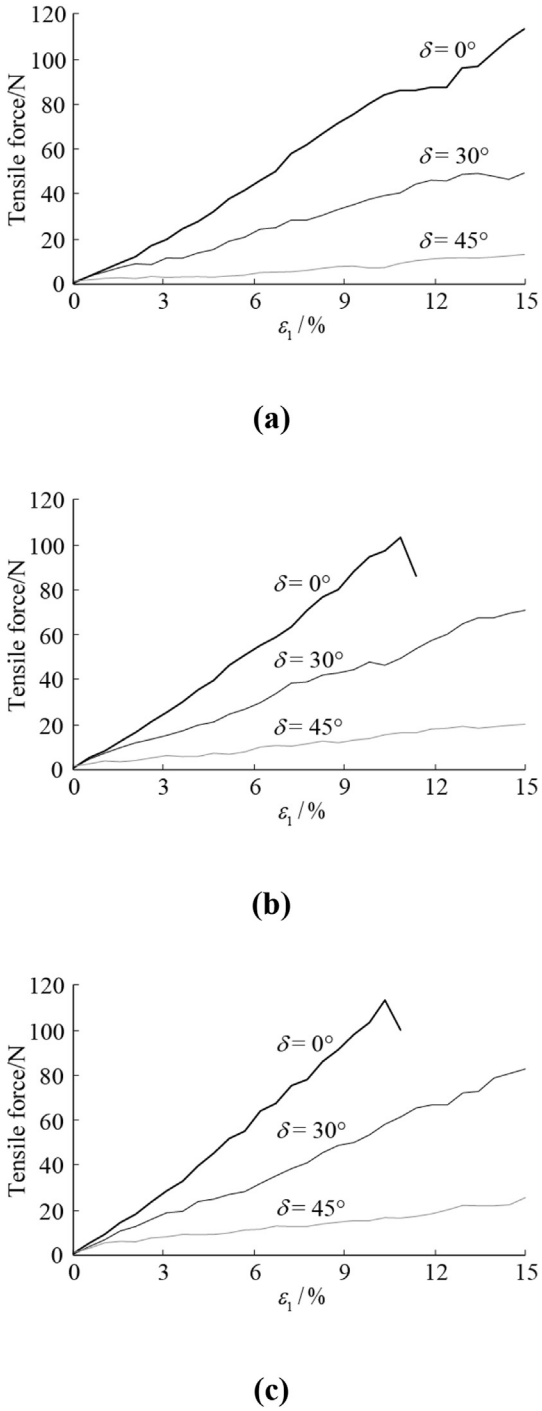

Fig. 12. Evolution of the tensile forces of the bags at different inclined angles during biaxial compression under three confining stresses: (a) σ_3 = 100 kPa; (b) σ_3 = 200 kPa; (c) σ_3 = 300 kPa.

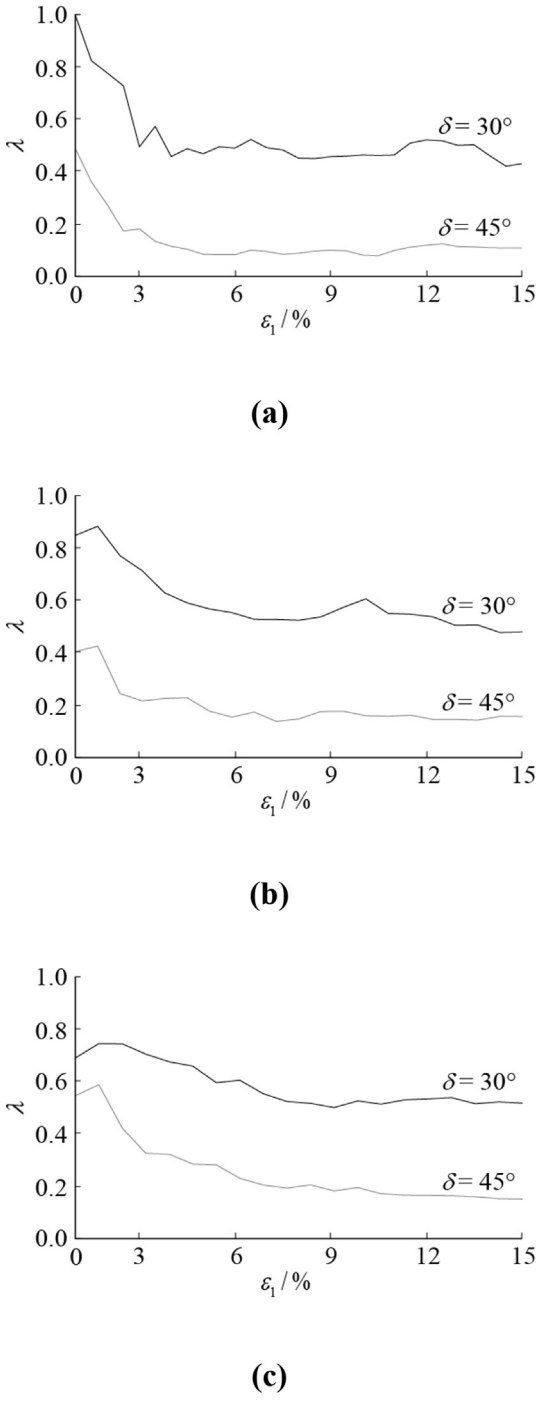

Fig. 13. Evolution of the normalized tensile forces of the bags in the cases of δ = 30° and 45°: (a) σ_3 = 100 kPa; (b) σ_3 = 200 kPa; (c) σ_3 = 300 kPa.

$$c_T = (m+1)\frac{T_v \cos 2\,\delta}{B}\tan\varphi_s + (m-1)\frac{T_v}{B}\frac{\cos^2 2\delta}{\cos\varphi_s} \tag{19}$$

Fig. 15 shows the variation of the apparent cohesions c_T of the soilbags with the inclined angle calculated from Eq. (19), together with the numerically simulated ones at five different inclined angles. In the calculation, the internal friction angle φ_s of the material inside the bags is taken as 24° and the tensile force T_v in the case of $\delta = 0°$ is taken as 110N (*see* Fig. 11). It can be seen that the predicted apparent cohesions c_T of the soilbags under inclined angles agree well with the numerically simulated ones, indicating the reasonability of Eq. (19).

5. Conclusion

In this paper, the strength characteristics of soilbags subjected not only to vertical loads but also to inclined loads were studied. A 2D strength formula of soilbags under inclined loads ($\delta \neq 0$) was derived, characterized as the apparent cohesion c_T of the soilbags

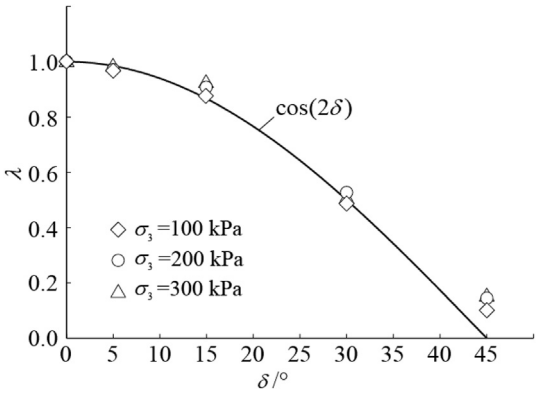

Fig. 14. The simulated reduction factors plotted against the inclined angles.

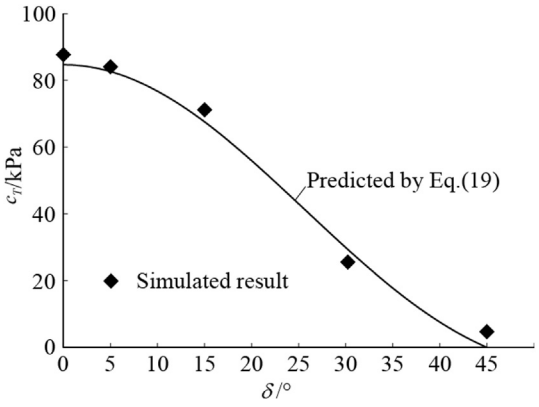

Fig. 15. Predicted and simulated apparent cohesion c_T of soilbags under inclined loads.

(Eq. (19)). The DEM simulation method for soilbags was proposed, in which the flexible bag was modeled as a series of small particles interconnecting with an elastic spring and a viscous dashpot when extended. The DEM simulation was conducted on the inclined assembly of soilbags under biaxial compression to verify the derived strength formula of soilbags. The main results are as follows:

(1) The confinement effect of the bag is quantified by the tensile force around its circumference. The developed tensile force of the bag decreases with the increasing inclination of the soilbag. Its reduction factor λ can be approximately expressed as a cosine function of the inclined angle δ.
(2) The high compressive strength of the soilbag can be interpreted as the contribution of an apparent cohesion resulting from the tensile force of the bag. In accordance with the variation of the bag's tensile force, the apparent cohesion of soilbags decreases with the increasing inclination of soilbags.
(3) The confinement effect of the bag is well modeled in the DEM simulation, indicating the effectiveness of the proposed simulation method for soilbags. It may also be used to simulate the earth reinforcement with other geosynthetics.
(4) The apparent cohesion of soilbags under different inclination can be reasonably predicted by Eq. (19). It is possible to take this apparent cohesion into account in the design of some soilbags-constructed projects, such as retaining walls et al.

Finally, it is worth mentioning that the study of the strength characteristics of soilbags under different inclination in this paper is undertaken in two dimensions. It is necessary to extend it to three dimensions for more reasonable assessment on the reinforcement effect of soilbags. And, further validations are also needed through laboratory experiments or numerical simulations.

Acknowledgements

The authors greatly appreciate the support provided by the National Natural Science Foundation of China (51379066), the Priority Academic Program Development of Jiangsu Higher Education Institutions (YS11001), the Fundamental Research Funds for the Central Universities (2015B25014) and Postgraduate Research & Practice Innovation Program of Jiangsu Province (SJCX17_0127). The authors are also grateful to Jiaorong Gao, Yang Lu, Kewei Fan, Jianlei Wang and Yingjun Song, the former or current students of Hohai University, for their great help in this study. The authors also appreciate the assessors' excellent comments and constructive suggestions to the study.

References

Ahmed, M.R., Tran, V.D.H., Meguid, M.A., 2015. On the role of geogrid reinforcement in reducing earth pressure on buried pipes: experimental and numerical investigations. Soils. Found. 55, 588–599.
Ansari, Y., Merifield, R., Yamamoto, H., Sheng, D.C., 2011. Numerical analysis of soilbags under compression and cyclic shear. Comput. Geotech. 38 (5), 659–668.
Bai, F.Q., Liu, S.H., Wang, Y.Q., 2010. Research on reinforcement mechanism and failure strength of soilbags. Rock Soil Mech. 31, 172–176 (in Chinese).
Bhandari, A., Han, J., 2010. Investigation of geotextile-soil interaction under a cyclic vertical load using the discrete element method. Geotext. Geomem 28, 33–43.
Bhandari, A., Han, J., Parsons, R.L., 2015. Two-dimensional DEM analysis of behavior of geogrid-reinforced uniform granular bases under a vertical cyclic load. Acta Geotech. 10 (4), 469–480.
Chen, C., Indraratna, B., McDowell, G., Rujikiatkamjorn, C., 2015. Discrete element modelling of lateral displacement of a granular assembly under cyclic loading. Comput. Geotech. 69, 474e484.
Cheng, H.Y., Yamamoto, H., Thoeni, K., 2016. Numerical study on stress states and fabric anisotropies in soilbags using the DEM. Comput. Geotech. 76, 170–183.
Cheng, H.Y., Yamamoto, H., Thoeni, K., Wu, Y., 2017. An analytical solution for geotextile-wrapped soil based on insights from DEM analysis. Geotext. Geomem 45 (4), 361–376.
Cundall, P.A., 1971. A computer model for simulating progressive, large scale movements in blocky rock systems Proceedings of the international symposium on rock fractures. Nancy, France II-8. 1–12.
Cundall, P.A., Strack, O.D.L., 1979. A discrete numerical model for granular assemblies. Geotechnique 29 (1), 47–65.
Hornsey, W.P., Carley, J.T., Coghlan, I.R., Cox, R.J., 2011. Geotextile sand container shoreline protection systems: design and application. Geotext. Geomembr. 29 (4), 425–439.
Indraratna, B., Biabani, M.M., Nimbalkar, S., 2014. Behavior of geocell-reinforced subballast subjected to cyclic loading in plane-strain condition. J. Geotech. Geoenviron. Eng. 141 (1), 04014081.
Kim, H.J., Won, M.S., Lee, K.H., Jamin, J.C., 2015. Model tests on dredged soil-filled geocontainers used as containment dikes for the Saemangeum reclamation project in South Korea. Int. J. Geomech. 16 (2), 04015055.
Kim, M., Freeman, M., FitzPatrick, B.T., Nevius, D.B., Plaut, R.H., Filz, G.M., 2004. Use of an apron to stabilize geomembrane tubes for fighting floods. Geotext. Geomembr. 22 (4), 239–254.
Lee, S.M., Choi, C., Shin, E.C., 2013. A study of connection stability for reinforced retaining wall constructed with soilbag with varying connection strength. J. Korean Geosynth. Soc. 12 (1), 101–107 (in Korean).
Li, Z., Liu, S.H., Wang, L.J., Zhang, C.C., 2013. Experimental study on the effect of frost heave prevention using soilbags. Cold Reg. Sci. Technol. 85, 109–116.
Liu, H.B., Yang, G.Q., Wang, H., Xiong, B.L., 2017. A large-scale test of reinforced soil railway embankment with soilbag facing under dynamic loading. Geomech. Eng. 12 (4), 579–593.
Liu, S.H., 2006. Simulating a direct shear box test by DEM. Can. Geotech. J. 43 (2), 155–168.
Liu, S.H., Bai, F.Q., Wang, Y.S., Wang, S., Li, Z., 2012. Treatment for expansive soil channel slope with soilbags. J. Aerosp. Eng. 26 (4), 657–666.
Liu, S.H., Gao, J.J., Wang, Y.Q., Weng, L.P., 2014. Experimental study on vibration reduction by using soilbags. Geotext. Geomembr. 42 (1), 52–62.
Liu, S.H., Lu, T.H., 2000. Microscopic shear mechanism of granular materials in simple shear by DEM. Chin. J. Geotech. Eng. 22 (5), 608–611 (in Chinese).
Liu, S.H., Lu, Y., Weng, L.P., Bai, F.Q., 2015. Field study of treatment for expansive soil/rock channel slope with soilbags. Geotext. Geomembr. 43 (4), 283–292.
Liu, S.H., Matsuoka, H., 2003. Microscopic interpretation on a stress-dilatancy relationship of granular materials. Soils Found. 43 (3), 73–84.
Liu, S.H., Matsuoka, H., 2007. A new earth reinforcement method by soilbags. Rock

Soil Mech. 28 (8), 1665–1670 (in Chinese).
Liu, S.H., Sun, D.A., 2002. Simulating the collapse of unsaturated soil by DEM. Int. J. Numer. Anal. Met. 26 (6), 633–646.
Liu, S.H., Xu, Y.F., 2001. Numerical simulation for a direct box shear test on granular material and microscopic consideration. Chin. J. Rock Mech. Eng. 20 (3), 288–292 (in Chinese).
Martinelli, L., Zanuttigh, B., De Nigris, N., Preti, M., 2011. Sand bag barriers for coastal protection along the Emilia Romagna littoral, Northern Adriatic Sea, Italy. Geotext. Geomembr. 29 (4), 370–380.
Matsuoka, H., Chen, Y., Kodama, H., Yamaji, Y., Tanaka, R., 2000a. Mechanical properties of soilbags and unconfined compression tests on model and real soilbags. Proc. of the 35th Japan National Conf. on Geotechnical Engineering. 544, 1075–1076 (in Japanese).
Matsuoka, H., Liu, S.H., 1999. Bearing capacity improvement by wrapping a part of foundation. Jpn. Soc. Civ. Eng. (JSCE), No.617/III-46 235–249 (in Japanese).
Matsuoka, H., Liu, S.H., 2003. New earth reinforcement method by soilbags ("Donow"). Soils Found. 43 (6), 173–188.
Matsuoka, H., Liu, S.H., 2006. A New Earth Reinforcement Method Using Soilbags. Taylor & Francis/Balkema, The Netherlands.
Matsuoka, H., Yamaguchi, K., Liu, S.H., Kodama, H., Yamaji, Y., 2000b. Construction cases of retaining walls and building foundation improvement by soilbags. Proc. of the 35th Japan National Conf. on Geotechnical Engineering. 545, 1077–1078 (in Japanese).
Matsuoka, H., Yamamoto, S., 1994. A microscopic study on shear mechanism of granular materials by DEM. Dob. Gakkai Ronbunshu 487, 167–175 (in Japanese).
Moreira, A., Vieira, C.S., das Neves, L., Lopes, M.L., 2016. Assessment of friction properties at geotextile encapsulated-sand systems' interfaces used for coastal protection. Geotext. Geomembr. 44 (3), 278–286.
Muramatsu, D., Zhang, F., Shahin, H.M., 2007. Numerical simulation on bearing capacity of soilbag-reinforced ground considering finite deformation. Jpn. Geotech. J. 2 (1), 11–23 (in Japanese).
Ngo, N.T., Indraratna, B., Rujikiatkamjorn, C., Biabani, M.M., 2015. Experimental and discrete element modeling of geocell-stabilized subballast subjected to cyclic loading. J. Geotech. Geoenviron. Eng. 142 (4), 04015100.
Tantono, S.F., Bauer, E., 2008. Numerical simulation of a soilbag under vertical compression. In: Proceedings of the 12th International Conference of International Association for Computer Methods and Advances in Geomechanics (IACMAG). Goa, India, pp. 433–439.
Wang, L.J., Liu, S.H., Zhou, B., 2015. Experimental study on the inclusion of soilbags in retaining walls constructed in expansive soils. Geotext. Geomembr. 43 (1), 89–96.
Wen, H., Wu, J.J., Zou, J.L., Luo, X., Zhang, M., Gu, C., 2016. Model tests on the retaining walls constructed from geobags filled with construction waste. Adv. Mater. Sci. Eng. 4971312.
Xu, Y.F., Huang, J., Du, Y.J., Sun, D.A., 2008. Earth reinforcement using soilbags. Geotext. Geomembr. 26 (3), 279–289.
Yamamoto, S., 1995. Fundamental Study on Mechanical Behavior of Granular Materials by DEM. Dr. Eng. Thesis. Nagoya Institute of Technology, Japan (in Japanese).
Ye, B., Muramatsu, D., Ye, G.L., Zhang, F., 2011. Numerical assessment of vibration damping effect of soilbags. Geosynth. Int. 18 (4), 159–168.

Notations

B: the width of the soilbag (m)
c_s: the cohesion of the wrapped soil (kPa)
c_T: the apparent cohesions of the soilbags under inclined angles (kPa)
H: the height of the soilbag (m)
k_n: the normal stiffness (N/m^2)
k_s: the tangent stiffness (N/m^2)
m: B/H
T: the bag tensile force (N)
T_v: the tensile force in the case of $= 0^\circ$ (N)
δ: the angle between the direction of the major principal stress σ_1 and the short axis of soilbag (°)
Δt: time step (s)
Δt_c: the critical time step (s)
ε_1: the vertical strain of the soilbags (%)
η_n: the normal damping (N·s/m^2)
η_s: The tangent damping (N·s/m^2)
λ: the reduction factors of the bag tensile force
$\boldsymbol{\sigma}$: the externally applied stress (kPa)
$\boldsymbol{\sigma_s}$: the stress of the soil wrapped in the bag (kPa)
$\boldsymbol{\sigma_T}$: the additional stress produced by the tension of the bag (kPa)
σ_{01}: the additional major principal stress produced by the tension of the bag (kPa)
σ_{03}: the additional minor principal stress produced by the tension of the bag (kPa)
σ_1: the vertical major principal stress of the soilbags (kPa)
σ_{1s}: the major principal stresses of the wrapped soil (kPa)
σ_3: the horizontal minor principal stress of the soilbags (kPa)
σ_{3s}: the minor principal stresses of the wrapped soil (kPa)
φ: the internal friction angle of the material inside the bags (°)
φ_s: the internal friction angle of the material inside the bags (°)